Research Square

Preprints are preliminary reports that have not undergone peer review.
They should not be considered conclusive, used to inform clinical practice,
or referenced by the media as validated information.

Development of an Automated Semiconductor Energy Band Gap Measurement Experiment with Fuzzy-PID Temperature Stabilization

Ahmad Radhy
ahmadradhy@its.ac.id

Institut Teknologi Sepuluh Nopember https://orcid.org/0009-0006-5104-294X

Rifky Firmansyah
Institut Teknologi Sepuluh Nopember

Dimas Dwi Firmansyah
Institut Teknologi Sepuluh Nopember

Herry Sufyan Hadi
Institut Teknologi Sepuluh Nopember https://orcid.org/0009-0006-9824-8726

Zulkaida Akbar
zulkaida.akbar@cern.ch

National Research and Innovation Agency (BRIN)

M Jauhar Kholili
National Research and Innovation Agency (BRIN)

Research Article

Keywords: energy band gap, fuzzy-PID control, automated measurement, laboratory experiment, quality education

Posted Date: August 13th, 2026

DOI: https://doi.org/10.21203/rs.3.rs-10679427/v1

License: This work is licensed under a Creative Commons Attribution 4.0 International License.
Read Full License

Additional Declarations: The authors declare potential competing interests as follows: No

Journal Name

PAPER

Development of an Automated Semiconductor Energy Band Gap Measurement Experiment with Fuzzy-PID Temperature Stabilization

Ahmad Radhy[1,*], Rifky Firmansyah[1],Dimas Dwi Firmansyah[1], Herry Sufyan Hadi[1], Zulkaida Akbar[2,*] and M Jauhar Kholili[2]

[1]Department of Instrumentation Engineering, Institut Teknologi Sepuluh Nopember, Surabaya, Indonesia
[2]Research Center for Quantum Physics, National Research and Innovation Agency (BRIN), Jakarta, Indonesia
*Author to whom any correspondence should be addressed.

E-mail: ahmadradhy@its.ac.id, zulkaida.akbar@cern.ch

Keywords: energy band gap, fuzzy-PID control, automated measurement, laboratory experiment, quality education

Abstract

Accurate determination of the semiconductor energy band gap is essential for understanding the electrical properties of semiconductor materials and represents a fundamental experiment in undergraduate solid-state physics laboratories. However, conventional laboratory methods are often constrained by unstable temperature conditions, limited measurement sensitivity, and fragmented experimental procedures, reducing both measurement accuracy and students' understanding of the relationship between semiconductor theory and experimental observations. This study presents the development of an automated laboratory platform for semiconductor energy band gap measurement based on current–voltage characterization with Fuzzy-PID temperature stabilization. The proposed system integrates automated temperature control, current–voltage data acquisition, real-time visualization, and digital data storage into a single experimental platform. Temperature stabilization was achieved using a Fuzzy-PID controller to minimize thermal fluctuations during measurement, thereby improving the reliability and repeatability of energy band gap determination. The system was experimentally validated using Silicon and Germanium diodes over a controlled temperature range. Compared with a conventional PID controller, the proposed Fuzzy-PID controller reduced the steady-state error from 1.67% to 0.65% at a 50°C setpoint and from 1.56% to 0.89% at an 80°C setpoint, resulting in improved thermal stability throughout the experiment. Using the forward-bias method, the measured energy band gap of Silicon ranged from (1.0601 ± 0.0072) eV to (1.0833 ± 0.0075) eV, in close agreement with the theoretical value of 1.1 eV. For Germanium, measured values of (0.7706 ± 0.1352) eV and (0.6170 ± 0.0755) eV were obtained under forward currents of 18 mA and 25 mA, respectively, closely matching the theoretical value of 0.67 eV. Overall, the developed system provides a reliable, cost-effective, and educationally effective platform for semiconductor energy band gap experiments while supporting undergraduate laboratory instruction and semiconductor characterization research.

1 Introduction

Semiconductor materials are the foundation of modern electronic and optoelectronic technologies. Their electrical behavior is primarily governed by the energy bandgap, which determines the minimum energy required for electrons to transition from the valence band to the conduction band, and consequently influences the electrical conductivity of the material [1, 2]. Because of its fundamental role in explaining the electrical properties of semiconductors, the concept of the energy band gap is an essential topic in undergraduate courses such as Solid-State Physics, Semiconductor Physics, and Electronic Materials. Laboratory experiments that enable students to directly observe the relationship between electrical characteristics and the energy bandgap are therefore indispensable for reinforcing theoretical concepts through practical investigations [3].

One of the most widely adopted experimental approaches for determining the semiconductor energy band gap is based on current–voltage (I–V) characterization, either through the analysis of reverse saturation current or forward-bias characteristics measured under controlled temperature conditions [4]. The accuracy of this method strongly depends on the precision of both the electrical and thermal measurements. In particular, for the forward-bias method, the applied temperature directly affects the forward voltage and shifts the I–V characteristics of semiconductor devices. These temperature-dependent changes alter the slope of the measured curve, which serves as the basis for estimating the energy bandgap. Consequently, inadequate temperature regulation introduces measurement uncertainty and reduces the reliability and repeatability of the calculated energy bandgap [5].

Several educational measurement systems have been developed to facilitate semiconductor bandgap experiments. For example, an AVR microcontroller-based instrument was designed to determine the energy band gaps of silicon and germanium diodes; however, data acquisition and analysis were performed separately, limiting the experimental efficiency [6]. Other studies have introduced educational laboratory kits with automated data recording to support student learning [3]. Although these systems simplify the experimental procedure, they generally pay limited attention to temperature stabilization, despite its significant influence on measurement accuracy. Recently, PID-based temperature controllers have been incorporated into sample holders for band gap measurements [4]. Nevertheless, conventional PID controllers often exhibit degraded performance under nonlinear operating conditions and parameter variations caused by changes in thermal dynamics [6]. Consequently, existing educational laboratory systems still lack an integrated platform capable of providing stable temperature regulation, automated current–voltage acquisition, and structured data management within a single experimental setup.

To address these limitations, this study presents the development of an automated laboratory experiment for semiconductor energy bandgap measurement that incorporates fuzzy-PID temperature stabilization. By combining the well-established control structure of PID with the adaptive reasoning capability of fuzzy logic, the proposed controller provides improved temperature stability while reducing the overshoot, steady-state error, and temperature fluctuations during measurement [7]. The automated system integrates temperature control, current and voltage acquisition, and data recording into a unified STM32-based platform, enabling reliable and repeatable bandgap measurements of silicon and germanium diodes. Beyond improving measurement accuracy, the proposed experiment is intended as an educational laboratory platform that enables students to investigate the relationship between temperature, current–voltage characteristics, and semiconductor energy bandgap through an automated and reproducible experimental procedure. Therefore, the objectives of this study are to develop an automated laboratory experiment, evaluate the performance of Fuzzy-PID temperature stabilization using standard control response metrics, and validate the system through energy band gap measurements of silicon and germanium semiconductor devices.

2 Experimental Setup

To support undergraduate laboratory instruction, a compact and portable experimental platform for semiconductor energy bandgap measurement was developed and evaluated in the Electronics Laboratory, Department of Instrumentation Engineering, Institut Teknologi Sepuluh Nopember (ITS). The system integrates a control unit for data acquisition and fuzzy-PID temperature regulation with a thermally controlled measurement chamber for semiconductor characterization. All electronic and mechanical components were housed in a custom 3D-printed enclosure, resulting in a robust and portable laboratory instrument that enables students to investigate the relationship between temperature and current–voltage characteristics of semiconductor devices while ensuring reliable and repeatable measurements. The overall system architecture is illustrated in Figure 1(a), and the complete experimental apparatus is shown in Figure 1(b).

2.1 Hardware Design

2.1.1 Chamber and Thermal Actuation

The measurement chamber was designed to provide a thermally stable environment for semiconductor energy bandgap experiments by minimizing heat exchange with the surroundings. The chamber was fabricated from polyethylene (PET) and internally lined with a thermal-insulating foam to reduce heat loss and maintain temperature uniformity. Temperature regulation was achieved using a thermoelectric module (TEC-12707) integrated with heat sinks and forced-air cooling, consisting of an internal circulation fan to ensure a uniform temperature distribution around the semiconductor sample and an external exhaust fan to dissipate excess heat.

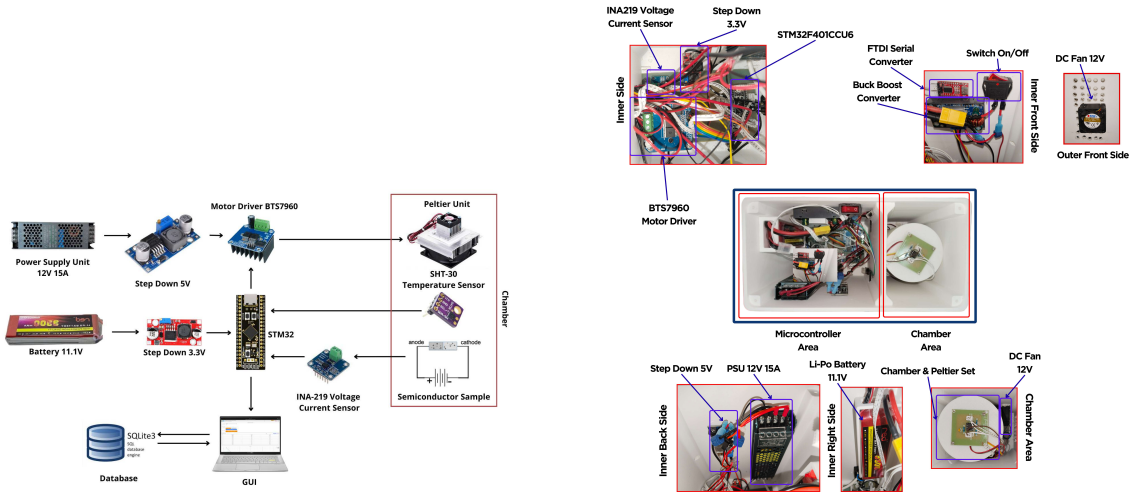


Figure 1. Experimental setup. (a) Hardware architecture. (b) Experimental apparatus.

An SHT-30 temperature sensor, positioned adjacent to the sample holder, continuously monitored the chamber temperature and provided feedback to the Fuzzy-PID controller, enabling stable temperature regulation with minimal fluctuations during the current–voltage characterization. The detailed configuration of the measurement chamber is shown in Figure 2.

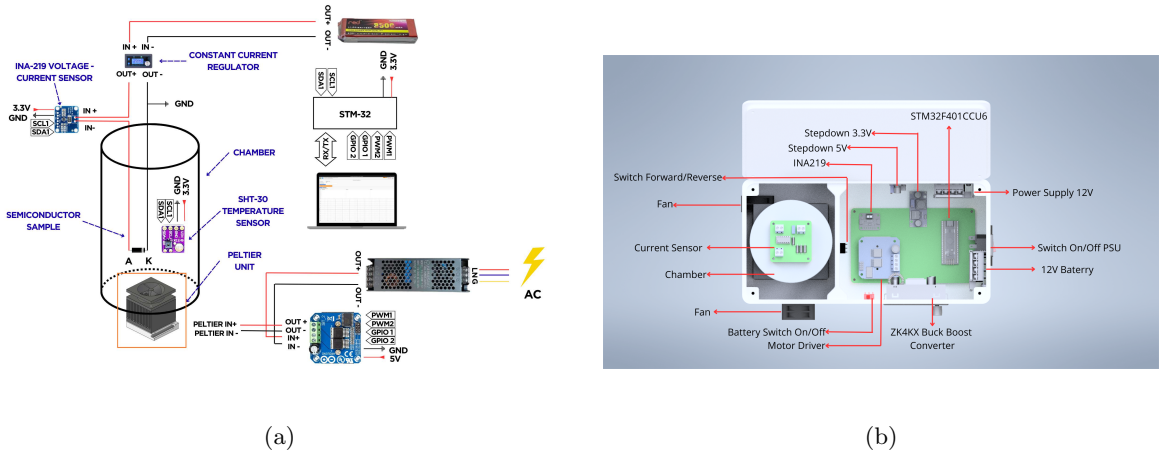


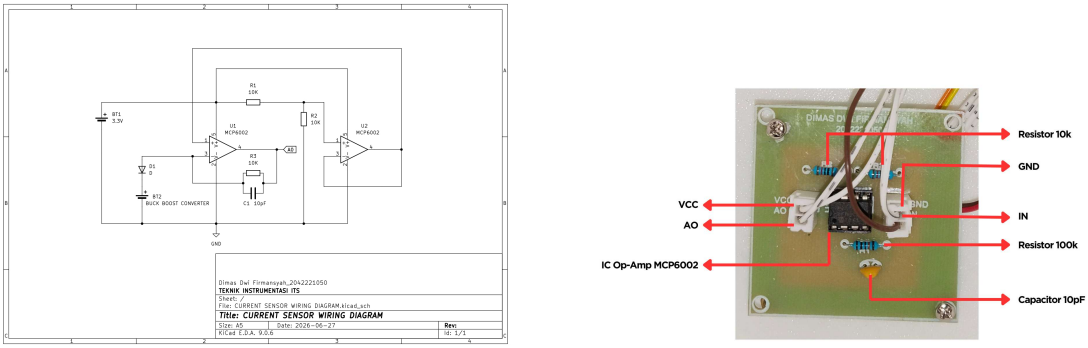
Figure 2. Experimental configuration of the semiconductor energy band gap measurement system. (a) Schematic of the forward-bias voltage measurement system, in which the semiconductor diode is placed inside a temperature-controlled chamber while a constant-current source and a Fuzzy-PID controller regulate the measurement conditions. (b) Three-dimensional (3D) design illustrating the internal component layout of the developed measurement system.

2.1.2 Control Unit and Power Management

The control unit, positioned outside the measurement chamber to minimize thermal interference, served as the central hub for system control, data acquisition, and power management. An STM32F401CCU6 microcontroller was used to coordinate the temperature regulation, acquire the sensor data, and communicate with the host computer throughout the experiment. To support both laboratory and portable operations, the system is powered by either a 12 V regulated power supply or an 11.1 V rechargeable battery, with onboard voltage regulation providing stable 5 V and 3.3 V supplies for the control and sensing circuits. Temperature regulation was achieved using a BTS7960 H-bridge driver, which adjusted the magnitude and polarity of the voltage applied to the thermoelectric (TEC-12707) module according to the Fuzzy-PID controller output, enabling bidirectional heating and cooling. For semiconductor characterization, a ZK-4KX buck–boost converter operated as a constant-current source, ensuring stable excitation during current–voltage measurements, thereby improving the measurement accuracy and repeatability.

2.1.3 Signal Acquisition Circuits

To accurately characterize the current–voltage behavior of the semiconductor device, the system incorporates dedicated voltage and current-sensing modules interfaced with the STM32 microcontroller. The forward and reverse voltages were measured using an INA219 sensor, which provided digital voltage data for real-time acquisition. In contrast, the reverse saturation current is typically in the nanoampere-to-microampere range [8], requiring high-sensitivity signal conditioning before measurement. Therefore, a nanoampere current sensor based on an MCP6002 operational amplifier configured as a transimpedance amplifier (TIA) was employed to convert the low-level current into a measurable voltage signal for the analog-to-digital converter (ADC) of the microcontroller [9]. The detailed circuit configuration for the reverse current measurement is shown in Figure 3.



(a) (b)

Figure 3. Current sensor implementation used for reverse current measurement. (a) Current sensor wiring diagram. (b) Fabricated MCP6002 current sensor printed circuit board (PCB).

2.2 Energy Band Gap Measurement

The energy bandgap of semiconductor materials based on p-n junction diodes can be determined by analyzing the current-voltage characteristics using two distinct approaches: the forward bias and reverse bias methods.

2.2.1 Forward Bias Method

In the forward-bias method, the semiconductor energy bandgap is determined from the temperature dependence of the diode forward voltage at a constant forward current. As the temperature increased, the forward voltage decreased systematically owing to changes in the semiconductor carrier concentration, providing the basis for estimating the energy bandgap. This relationship is described by the fundamental current–voltage equation of a p–n junction diode:

$$I = C \exp\left(\frac{eV - E_g}{\eta k_B T}\right) \tag{1}$$

Equation 1 indicates that the diode current depends exponentially on the applied voltage (V) and temperature (T). Because the pre-exponential term contains material-dependent parameters, including the energy bandgap (E_g) [3], the equation can be rearranged to isolate the exponential component, thereby facilitating the derivation of the bandgap expression. Dividing both sides of the equation by the pre-exponential constant C yields:

$$\frac{I}{C} = \exp\left(\frac{eV - E_g}{\eta k_B T}\right) \tag{2}$$

To linearize this relationship, a natural logarithm was applied to both sides, which was then simplified by utilizing the inverse property of logarithmic and exponential functions:

$$\ln\left(\frac{I}{C}\right) = \ln\left(e^{\frac{eV - E_g}{\eta k_B T}}\right) \tag{3}$$

The resulting expression is subsequently multiplied by the thermal energy term to eliminate the denominator:

$$\eta k_B T \ln\left(\frac{I}{C}\right) = eV - E_g \tag{4}$$

Finally, the terms are rearranged into the linear form presented below:

$$eV = E_g + \eta k_B T \ln\left(\frac{I}{C}\right) \tag{5}$$

Based on the resulting linear equation 5, the semiconductor energy bandgap was determined from the intercept of the linear regression between the measured temperature and diode voltage. Because the forward-bias method required a constant forward current throughout the experiment, a ZK-4KX buck–boost converter was employed as a constant-current source to ensure stable excitation during the measurement process.

To quantify the uncertainty of the estimated energy bandgap, an uncertainty propagation analysis was performed based on the intercept obtained from the linear regression of the voltage–temperature characteristics [10]. Because the intercept is directly related to the extrapolated bandgap value, its uncertainty provides an important indicator of the reliability of the estimated energy bandgap [10]. In linear regression, this uncertainty is represented by the standard error of the intercept, which quantifies the statistical uncertainty of the fitted parameter arising from the experimental data dispersion rather than the variability of the measured data itself. The standard error of the intercept SE_b was calculated using Equation 6 according to the formulation in [11]:

$$SE_b = \sigma\sqrt{\frac{1}{n} + \frac{\bar{x}^2}{S_{xx}}} \tag{6}$$

The calculated standard error was subsequently propagated to determine the uncertainty of the energy bandgap (ΔE_g), providing a quantitative estimate of the confidence associated with the extracted bandgap values. This analysis enables a more rigorous evaluation of the measurement reliability and strengthens the comparison of the silicon and germanium energy band gaps under different temperature conditions.

2.2.2 Reverse Bias Method

Alternatively, under reverse-bias conditions, a semiconductor diode produces a small reverse-saturation current generated by thermally excited minority charge carriers. Because the concentration of these carriers varies significantly with temperature, the reverse saturation current exhibits a pronounced temperature dependence. This behavior forms the basis for estimating the semiconductor energy band gap, and the relationship between the reverse saturation current (I_r), energy band gap (E_g), and the absolute temperature (T) is expressed by the following equation 7 [2]:

$$I_r = A \exp\left(-\frac{E_g}{\eta k_B T}\right) \tag{7}$$

In this equation, A is the material constant, k_B is the Boltzmann constant (8.617×10^{-5} eV/K), and η is the diode quality factor $\eta = 1$ for Germanium; $\eta = 2$ for Silicon). To determine the value of E_g experimentally, the equation is linearized using the natural logarithm (ln) to become:

$$\ln(I_r) = \ln(A) - \frac{E_g}{\eta k_B T} \tag{8}$$

The acquired data were processed by plotting ln (I_r) as a function of $(1/\mathrm{T})$, producing a linear relationship with a slope (m). The slope obtained from the linear regression was subsequently used to calculate the semiconductor energy bandgap according to the following equation 9:

$$E_g = -\eta k_B m \tag{9}$$

For the reverse-bias method, the uncertainty of the estimated semiconductor energy bandgap (E_g) was evaluated to assess the accuracy and reliability of the measurement results [2]. Because E_g is determined from the slope of the linear regression between ln (I_r) and $1/T$, it is expressed by the following equation 10:

$$y = a + mx \tag{10}$$

where $y = \ln(I_r)$, $x = 1/T$, and m is the slope of the regression line. Because the semiconductor energy bandgap E_g is directly proportional to the slope, its uncertainty is determined by the uncertainty associated with m. This uncertainty was evaluated from the residual error, defined as the deviation of each experimental data point from the fitted regression line:

$$e_k = y_k - f(x_k) \tag{11}$$

The variance of the residuals was then calculated as:

$$s^2 = \frac{1}{n-2} \sum_{k=1}^{n} e_k^2 \tag{12}$$

where n is the number of observations. Based on the least squares fitting method, the uncertainty of the slope is represented by the standard error:

$$\delta m = \frac{s}{\sqrt{S_{xx}}} \tag{13}$$

with:

$$S_{xx} = \sum_{k=1}^{n} (x_k - \bar{x})^2 \tag{14}$$

The uncertainty of the energy band gap is then propagated from the slope uncertainty as:

$$\delta E_g = \eta k_B \, \delta m \tag{15}$$

Thus, the final energy band gap result can be expressed as: $E_g \pm \delta E_g$, where δE_g represents the uncertainty range of the measured energy band gap. A smaller δm indicates better agreement between the experimental data and the linear regression model, resulting in a more reliable E_g estimation [2].

2.3 Open Loop Test and Default PID Tuning

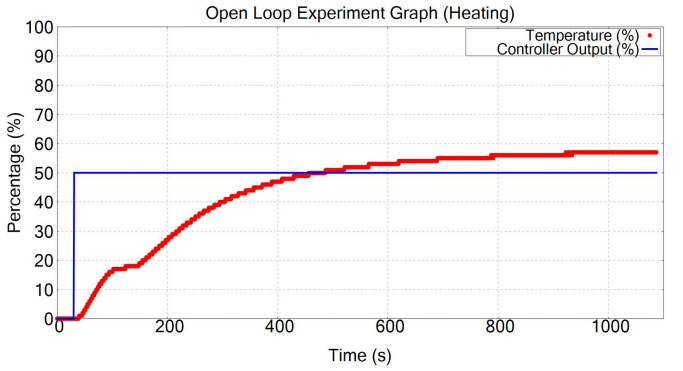
The chamber temperature was regulated using a Fuzzy-PID controller. An SHT-30 temperature sensor continuously monitored the chamber temperature and provided feedback for comparison with the desired set point. Based on the resulting control error, the controller adjusted the magnitude and polarity of the voltage applied to the thermoelectric (Peltier) module to regulate the temperature of the chamber. In this control scheme, the thermal output of the Peltier module served as the manipulated variable, whereas the chamber temperature was maintained as the controlled variable. The bidirectional heating and cooling capability of the Peltier module, achieved by simply reversing the applied voltage polarity, makes it well-suited for applications requiring precise temperature regulation [12].

Table 1. Default PID parameters for cooling and heating processes utilized as the initial reference for the Fuzzy PID control system.

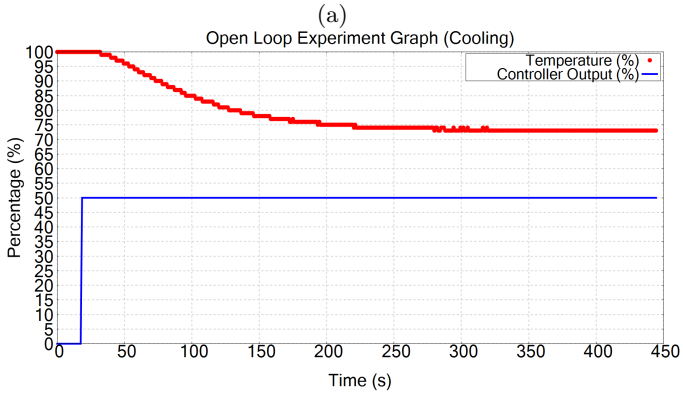
PID Paramters	Cooling Process	Heating Process
K_p	1.0	1.5
K_i	2.0	2.5
K_d	3.0	3.5

Before implementing the fuzzy-PID controller, the process dynamics were first identified to obtain suitable initial PID parameters [13]. Open-loop experiments were conducted without feedback under both heating and cooling operating modes to characterize the thermal response of the chamber [14]. The experimental data were subsequently approximated using a first-order plus dead time (FOPDT) model, from which the initial PID parameters were determined using the Ziegler–Nichols tuning method. The resulting open-loop responses are shown in Figure 4.

Experimental characterization showed that the thermoelectric actuator provided an operating temperature range of 12.8 °C to 96.2 °C, with a transition temperature of 34 °C corresponding to the thermal equilibrium condition measured in a non-air-conditioned environment, while the controller remained inactive. During the open-loop tests, the controller output was initially maintained at 50%, followed by a step increase to 75% to evaluate the dynamic response of the



(a)



(b)

Figure 4. Open-loop response characteristics of the system for (a) heating and (b) cooling modes. The graphs illustrate the dynamic temperature response (red line) following a step change in the controller output (blue line) from 0% to 50%. It is observed that the heating process reaches a steady-state value of approximately 57% over a longer duration, whereas the cooling process stabilizes at approximately 73% with a faster response time.

system. Based on the open-loop experimental results, the thermal dynamics of the system were approximated using first-order plus dead-time (FOPDT) models, represented by Equations 16 and 17 for the cooling and heating processes, respectively. These models were subsequently used to estimate the initial PID tuning parameters, which are listed in Table 1.

$$G(s) = \frac{0.54\, e^{-13.4s}}{160.6s + 1} \tag{16}$$

$$G(s) = \frac{1.12\, e^{-8.3s}}{472s + 1} \tag{17}$$

The initial PID parameters obtained from the identified FOPDT models were used as the starting values for the Fuzzy-PID temperature controller. To accommodate the nonlinear thermal behavior of the measurement chamber, the proportional K_p, integral K_i, and derivative K_d gains were adaptively adjusted in real time according to the control error and its rate of change through a fuzzy inference mechanism. This adaptive tuning strategy improved the robustness of the controller by reducing the overshoot and shortening the settling time under varying thermal loads and environmental disturbances. Consequently, stable and precise temperature regulation was achieved, providing reliable thermal conditions for semiconductor energy bandgap measurements.

2.4 Fuzzy Logic Design

The fuzzy inference engine processes the input variables through three sequential stages: fuzzification, rule evaluation, and defuzzification. During fuzzification, the crisp error and change-of-error signals are mapped into fuzzy sets using predefined membership functions. The fuzzy rule base then evaluates the corresponding linguistic rules to determine the appropriate control action, after which the inferred fuzzy output is converted into a crisp control signal through defuzzification [15]. The control strategy was mathematically represented by the conventional PID model given in Equation 18, whereas the adaptive fuzzy-PID controller was formulated by Equation 19 [16].

Table 2. Definition of linguistic labels and their corresponding numerical intervals utilized for the fuzzy membership functions.

Value	Description	Heating Interval
NB	Negative Big	[-3 -3 -2]
NM	Negative Medium	[-3 -2 -1]
NS	Negative Small	[-2 -1 0]
N	Normal	[-1 0 1]
PS	Positive Small	[0 1 2]
PM	Positive Medium	[1 2 3]
PB	Positive Big	[2 3 3]

$$U_{PID'} = K_P E + K_I \int E\,dt + K_D \frac{dE}{dt} \tag{18}$$

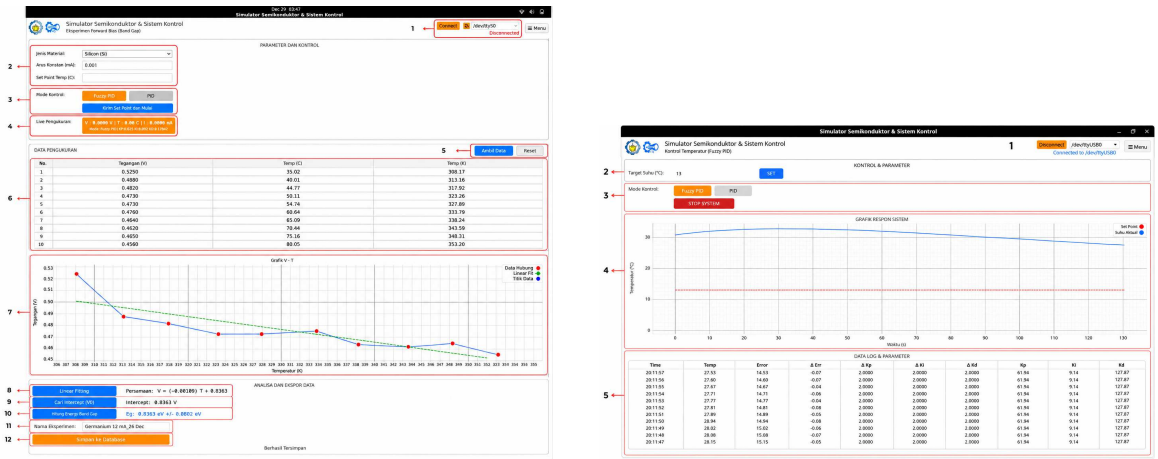
$$U'_{\text{PID–FZ}} = K_{\text{P–FZ}}\,E + K_{\text{I–FZ}} \int E\,dt + K_{\text{D–FZ}} \frac{dE}{dt} \tag{19}$$

The fuzzy inference system implemented in this study was adapted from the framework proposed in a previous study [17] to enable the adaptive tuning of the PID gains. The controller employed two input variables: the error (e), defined as the difference between the measured temperature and the desired setpoint, and the change in error (Δe), representing the variation between the current and previous error values [17]. These variables were processed using a fuzzy inference engine to determine the appropriate gain adjustments during temperature regulation.

The fuzzy model generated three incremental outputs, denoted as ΔK_p, ΔK_i and ΔK_d. These incremental adjustments were subsequently added to the initial K_p, K_i, and K_d parameters, which were determined through a preliminary tuning process. By integrating the fuzzy logic model into the control architecture, the system can dynamically update its parameters in response to the nonlinear thermal characteristics of the plant.

The membership functions for the error and delta error inputs are categorized into seven linguistic labels, which are distributed across a normalized interval ranging from -3 to 3. Similarly, the membership functions for the output variables ΔK_p, ΔK_i and ΔK_d were partitioned into seven linguistic terms within the same numerical range. This symmetrical distribution of the membership functions allows for a granular classification of the input-output relationships. The details of the fuzzy membership function for both the input and output are listed in Table 2.

2.5 Graphical User Interface



(a) (b)

Figure 5. Graphical user interfaces of the developed automated measurement system. (a) Main dashboard for semiconductor energy band gap analysis, including data acquisition, visualization, and energy band gap calculation. (b) Temperature control interface for configuring the Fuzzy-PID controller and monitoring the real-time thermal response of the measurement chamber.

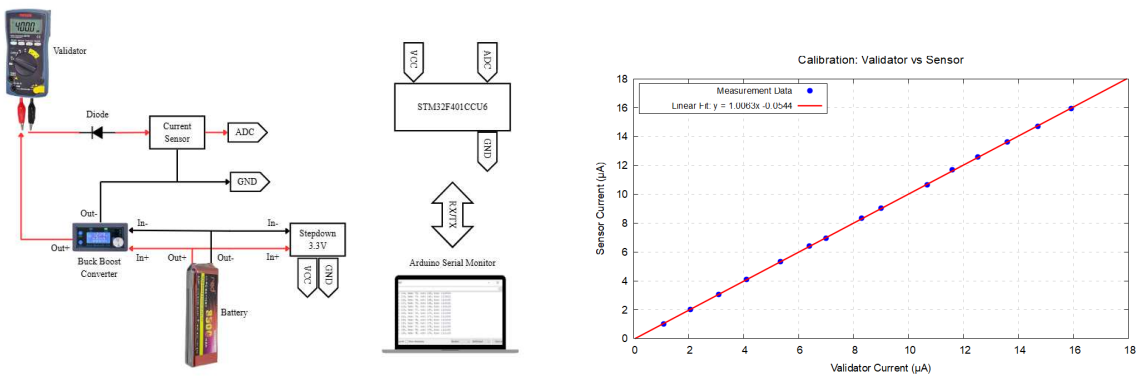
Figure 5 presents the graphical user interface, which is organized into 12 functional sections to support the complete experimental workflow. The experiment began by establishing serial

communication (label 1), followed by the configuration of measurement parameters, including the semiconductor material selection, constant-current input, and temperature setpoint (label 2). The desired control mode was then selected, and the fuzzy-PID controller was activated (label 3), while the real-time responses of the temperature, voltage, and current were continuously monitored (label 4). After thermal stabilization, the measurement data were manually acquired (label 5), stored in the data table (label 6), and automatically displayed on the plotting interface (label 7). Finally, the recorded data were processed through linear regression (label 8), intercept analysis (label 9), and energy band gap calculation with uncertainty estimation (label 10) before the experiment was finalized by assigning a measurement name (label 11) and storing the results in the database (label 12).

3 Results

3.1 Sensor Validation and Calibration

Before performing the semiconductor energy band gap characterization, the measurement system was validated and calibrated to ensure the accuracy and reliability of the acquired electrical-signal measurements. The calibration procedure was conducted by comparing the instrument outputs with those of a Sanwa CD770 digital multimeter 6 (a), which served as a reference instrument. The INA219 voltage sensor initially exhibited a measurement error of 0.72%. After applying a linear regression-based calibration, the error was reduced to 0.06%, corresponding to an accuracy of 99.94% relative to the reference values. Similarly, the MCP6002-based nanoampere current sensor, developed to measure the reverse saturation current, initially produced an error of 1.99%, which decreased to 1.37% following calibration, yielding an accuracy of 98.63%. These results demonstrate that the calibration procedure substantially improved the measurement performance of both sensing modules, enabling the reliable detection of low-level current signals during the reverse-bias experiment. The linearity of the calibrated nanoampere current sensor with respect to the reference instrument is shown in Figure 6 (b).



(a) (b)

Figure 6. Validation and calibration of the MCP6002-based nanoampere current sensor. (a) Experimental setup used to validate the MCP6002 current sensor against the reference digital multimeter. (b) Calibration results showing the linear relationship between the developed current sensor and the reference instrument, demonstrating the improved measurement accuracy after calibration.

3.2 Temperature Control System Performance Test

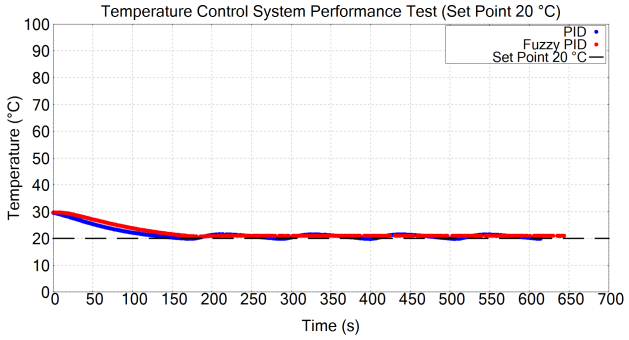
The performance of the proposed fuzzy-PID temperature controller was evaluated by comparing its transient and steady-state responses with those of a conventional PID controller. Five standard control performance indices, namely rise time, peak time, maximum overshoot, settling time, and steady-state error, were used to assess the performance of the controller. Experiments were conducted at temperature setpoints of 20, 50, and 80°C, with each response monitored for 600 s to ensure that steady-state conditions were achieved. The corresponding temperature response curves are shown in Figures 7(a)–(c).

Figure 7(a) shows the temperature response at a 20°C setpoint. Under these operating conditions, the conventional PID controller achieved stable temperature regulation, exhibiting a rise time of 117 s, settling time of 279 s, maximum overshoot of 0.8%, and steady-state error of 0.22%. In contrast, the Fuzzy-PID controller failed to reach the desired setpoint, stabilizing at

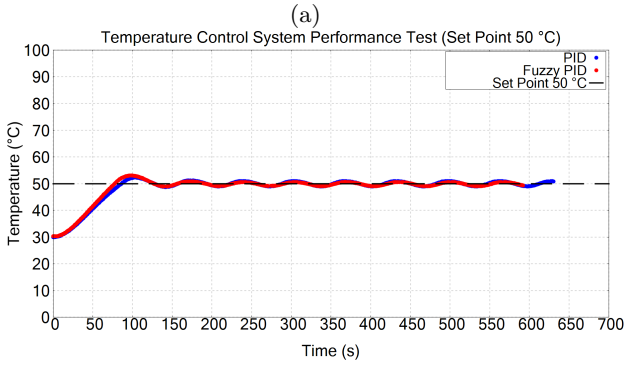
approximately 21°C. This result indicates that the proposed controller was less effective under low-temperature-cooling conditions.

The responses obtained at a 50°C setpoint are shown in Figure7(b). Compared with the conventional PID controller, the fuzzy-PID controller produced a faster transient response, reducing the rise time from 59 to 52 s and the peak time from 102 to 98 s. Although the maximum overshoot increased slightly from 4.54% to 6.08%, the steady-state error decreased substantially from 1.67% to 0.65%, and the settling time remained nearly unchanged. These results indicate that the adaptive gain adjustment improved the temperature tracking accuracy without compromising the system stability.

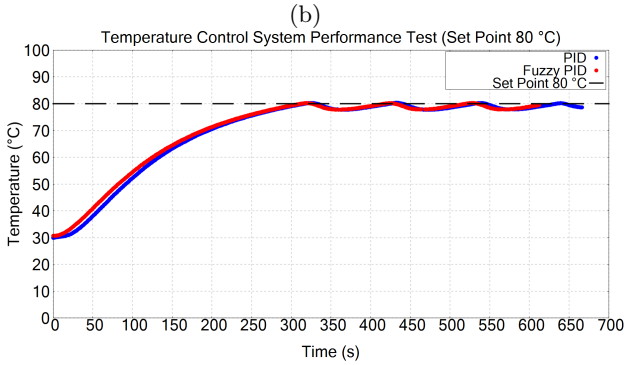
Figure 7(c) shows the temperature response at the 80°C setpoint. Both controllers exhibited comparable transient characteristics; however, the Fuzzy-PID controller achieved a lower maximum overshoot (0.30% versus 0.37%), shorter peak time, and reduced steady-state error (0.89% versus 1.56%). Although the improvement in rise and settling times was marginal, the reduction in steady-state error demonstrated that the adaptive Fuzzy-PID controller provided more accurate temperature regulation at medium and high operating temperatures. Nevertheless, its inferior performance at the 20°C setpoint suggests that further refinement of the fuzzy membership functions or control rules is required to improve low-temperature operation.



(a)



(b)



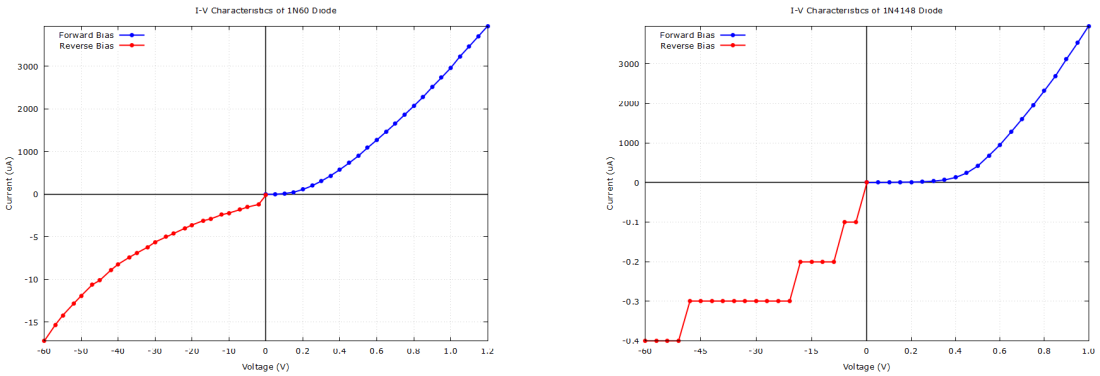
(c)

Figure 7. Performance comparison between the conventional PID and proposed Fuzzy-PID temperature control systems under different temperature setpoints. (a) Temperature regulation at a setpoint of 20°C. (b) Temperature regulation at a setpoint of 50°C. (c) Temperature regulation at a setpoint of 80°C. Each graph illustrates the transient and steady-state responses of both controllers during a 600 s temperature regulation test.

3.3 Current-Voltage (I-V) Characterization

Figure 8 presents the measured current–voltage (I–V) characteristics of (a) germanium and (b) silicon diodes prior to the energy bandgap determination. I–V characterization was performed to verify the electrical behavior of both semiconductor devices and to confirm their suitability for subsequent band gap measurements [18]. Under forward-bias conditions, the 1N60 germanium diode began conducting at a threshold voltage of approximately 0.15–0.25 V, whereas the 1N4148 silicon diode exhibited a higher threshold voltage of approximately 0.6–0.7 V, consistent with the larger energy bandgap of silicon.

Under reverse-bias conditions, neither diode exhibited a sudden increase in current up to the maximum applied voltage of 60 V, indicating that the breakdown region was not reached during the experiment. Instead, both devices maintained a stable reverse saturation current, which was dominated by thermally generated minority carriers. This stable reverse-bias behavior confirms that the measured microampere-level currents are sufficiently reliable for the subsequent extraction of the semiconductor energy bandgap.

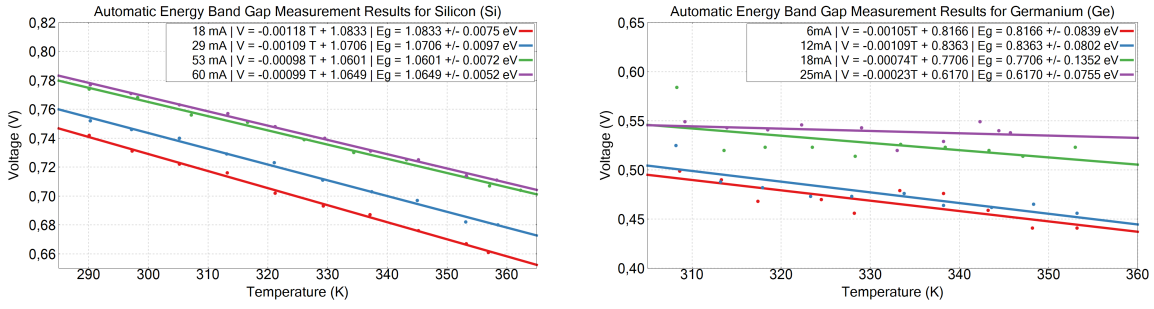


(a) (b)

Figure 8. Measured current–voltage (I–V) characteristics of the semiconductor devices used in this study. (a) I–V curve of the 1N60 Germanium diode. (b) I–V curve of the 1N4148 Silicon diode. The curves illustrate the forward- and reverse-bias electrical characteristics prior to energy band gap determination.

3.4 Forward Bias Energy Band Gap Measurement

This subsection presents the results of the semiconductor energy bandgap measurements obtained using the forward-bias method. To evaluate the consistency and repeatability of the proposed instrumentation system, measurements were performed under four constant current conditions. The corresponding voltage–temperature relationships for the Silicon and Germanium diodes are presented in Figures 9 (a) and (b), respectively, and the resulting data were analyzed using linear regression to determine the energy band gap.



(a) (b)

Figure 9. Voltage–temperature characteristics obtained from the automated forward-bias energy band gap measurement system. (a) Plot of forward voltage (V) versus temperature (°C) for the Silicon diode. (b) Plot of forward voltage (V) versus temperature (°C) for the Germanium diode. The measured data were subsequently analyzed using linear regression to determine the semiconductor energy band gap.

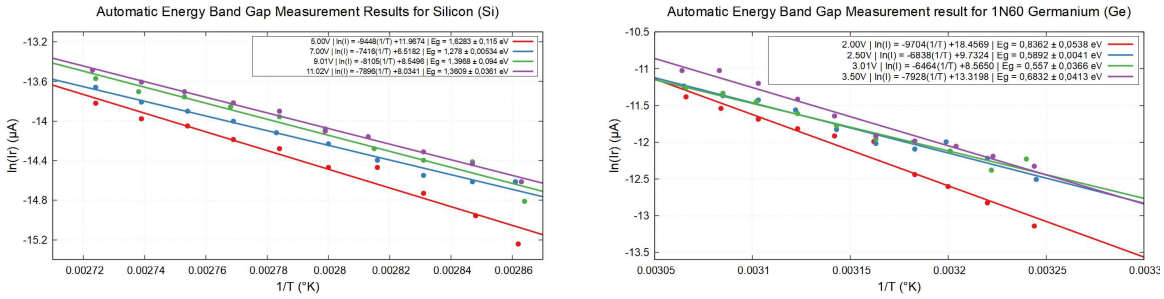
As shown in Figure 9 (a), the silicon diode exhibited a nearly linear decrease in the forward voltage with increasing temperature over the range of 290.1–362.3 K. The extracted energy band

gap values were 1.0833 ± 0.0075 eV at 18 mA, 1.0706 ± 0.0097 eV at 29 mA, 1.0601 ± 0.0072 eV at 53 mA, and 1.0649 ± 0.0052 eV at 60 mA. The relatively small variation among these results indicates good measurement consistency under different constant-current conditions.

Similarly, Figure 9 (b) shows an approximately linear voltage–temperature relationship for the Ge diode over the temperature range of 308.2–353.2 K. The calculated energy band gap values were 0.8166 ± 0.0839 eV at 6 mA, 0.8363 ± 0.0802 eV at 12 mA, 0.7706 ± 0.1352 eV at 18 mA, and 0.6170 ± 0.0755 eV at 25 mA. Although the estimated values exhibited greater variation than those obtained for silicon, the overall results remained within the expected range for germanium, confirming the capability of the developed automated measurement system to characterize semiconductor materials using the forward-bias method.

3.5 Reverse Bias Energy Band Gap Measurement

The reverse-bias method was subsequently employed to determine the energy bandgap of the Silicon and Germanium diodes using the developed automated measurement system. To evaluate the consistency and repeatability of the proposed instrumentation system, measurements were performed under four constant-voltage conditions. The corresponding linear regression plots of $(ln(I_r))$ versus $(1/T)$, from which the regression slope was obtained for the energy band gap calculation, are presented in Figures 10 (a) and (b). The strong linear relationships observed in both plots confirm the expected temperature dependence of the reverse saturation current and demonstrate the consistency of the experimental data acquired.



(a) (b)

Figure 10. Linear regression plots used for reverse-bias energy band gap determination based on the automated measurement system. (a) Plot of the natural logarithm of the reverse saturation current, $\ln(I_r)$, versus the reciprocal absolute temperature, $1/T$, for the Silicon diode. (b) Plot of $\ln(I_r)$ versus $1/T$ for the Germanium diode. The slope of each fitted line was used to calculate the corresponding semiconductor energy band gap.

As shown in Figure 10 (b), the measured energy bandgap values for the Ge diode ranged from 0.557 to 0.8362 eV. The average value obtained from all measurements was 0.666 eV, which is in excellent agreement with the theoretical band gap of approximately 0.67 eV. This close agreement indicates that the developed instrumentation system can accurately characterize Ge using the reverse-bias technique.

For the Silicon diode, the calculated energy bandgap values ranged from 1.278 to 1.6283 eV, as illustrated in Figure 10 (a). Although these values were consistently higher than the theoretical band gap of approximately 1.11 eV, the measurements exhibited excellent repeatability and low uncertainties. In particular, the measurement performed under the 7 V reverse-bias condition yielded an energy band gap of 1.278 eV with an uncertainty of only 0.00534 eV, demonstrating the high stability and sensitivity of the developed instrumentation system for measuring microampere-level reverse-saturation currents.

4 Discussion

4.1 Comparison of Transient and Steady-State Response Characteristics

The inability of the proposed Fuzzy-PID controller to achieve the 20°C setpoint can be attributed to the adaptive reduction of the integral gain as the temperature approached the target value. According to the classical control theory, the integral term accumulates residual errors to eliminate the steady-state error completely. However, the fuzzy inference mechanism progressively reduced the (K_i) gain in response to decreasing error and error variation, thereby weakening the controller's ability to compensate for residual thermal disturbances from the surrounding environment. Consequently, the control action became insufficient to overcome the remaining

temperature offset, causing the system to stabilize before reaching the desired setpoint [6]. By contrast, the conventional PID controller maintained a constant integral gain throughout the control process, allowing the accumulated integral action to continuously compensate for the residual error. Consequently, the conventional PID controller successfully reached the 20°C setpoint and maintained stable operation under the tested conditions [19].

Different control characteristics were observed at higher temperature setpoints. At 50°C, the fuzzy-PID controller produced a faster transient response and a lower steady-state error than the conventional PID controller, although this improvement was accompanied by a slightly larger overshoot. This behavior indicates that the fuzzy inference system temporarily increased the proportional gain to accelerate the temperature increase, resulting in a stronger initial control action before the adaptive mechanism gradually reduced the control effort as the setpoint was approached. At the 80°C setpoint, the conventional PID controller exhibited a slightly faster overall response, whereas the fuzzy-PID controller achieved superior steady-state performance by producing a lower overshoot and smaller steady-state error. This improvement can be explained by the adaptive adjustment of the controller gains, in which the fuzzy rule base increases the derivative gain while reducing the proportional gain near the target temperature, thereby providing additional damping and suppressing excessive oscillations during the final stage of the temperature regulation process [6].

4.2 Extraction and Validation of Forward Bias Energy Band Gap Values

The forward-bias measurements demonstrated that the developed instrumentation system was capable of producing energy bandgap values that closely matched the theoretical characteristics of both semiconductor materials. For the Silicon diode, the extracted energy band gap ranged from 1.0601 to 1.0833 eV under constant-current conditions of 18–60 mA, corresponding to an average deviation of approximately 4% from the theoretical value of 1.1 eV. Similarly, the Ge diode yielded energy band gap values between 0.6170 and 0.8363 eV over current variations of 6–25 mA, with the closest agreement to the theoretical value of 0.67 eV obtained at 25 mA [20]. These results indicate that the proposed fuzzy-PID temperature control system maintained sufficiently stable thermal conditions to preserve the linear voltage–temperature relationship required for reliable forward-bias energy band gap extraction, consistent with the theoretical requirement that accurate temperature regulation is essential for semiconductor band gap measurements [4].

Reverse-bias measurements further verified the capability of the developed system to characterize semiconductor materials through the temperature dependence of the reverse saturation current. The accurate measurement of microampere-level currents using the MCP6002-based transimpedance amplifier ensured reliable logarithmic regression of $\ln(I_r)$ versus $(1/T)$, thereby improving the accuracy of the extracted energy bandgap values. For the Ge diode, the average energy bandgap of 0.666 eV showed excellent agreement with the theoretical value of 0.67 eV [20]. In contrast, the silicon diode consistently produced values of approximately 1.278 eV, which were higher than the theoretical value of 1.11 eV [20]. Nevertheless, the consistently low measurement uncertainty, reaching $\pm$ 0.00534 eV under the 7 V reverse-bias condition, demonstrates the high precision and repeatability of the developed instrumentation. Collectively, these findings confirm that stable temperature regulation effectively preserves the linear relationship between $\ln(I_r)$ and $(1/T)$, thereby providing a reliable basis for the automated determination of the semiconductor energy band gap.

5 Conclusion

In this study, we successfully developed and validated an automated instrumentation system with fuzzy-PID temperature stabilization for semiconductor energy bandgap measurements. The integrated hardware demonstrated high measurement reliability, with the INA219 voltage sensor and MCP6002-based transimpedance amplifier achieving accuracies of 99.94% and 98.63%, respectively, relative to the reference instrument. The proposed Fuzzy-PID controller effectively regulated the nonlinear thermal dynamics of the measurement chamber, providing improved temperature stability, reduced overshoot, and lower steady-state error at the 50°C and 80°C setpoints compared with the conventional PID controller. The resulting stable thermal environment enabled an accurate determination of the energy bandgap using both forward- and reverse-bias characterization methods. The forward-bias measurements produced energy band gap values of approximately 1.06–1.08 eV for silicon and 0.617 eV for germanium, while the reverse-bias method yielded an average value of 0.666 eV for germanium, in close agreement with the theoretical value of 0.67 eV, and stable measurements of approximately 1.278 eV for silicon with very low uncertainty. Overall, the integration of precise current sensing, adaptive temperature

regulation, automated data acquisition, and graphical analysis provides a reliable and cost-effective experimental platform for semiconductor laboratory education, practical experimentation, and future semiconductor characterization.

Acknowledgments
This research is funded by Institut Teknologi Sepuluh Nopember (ITS) and managed under the Strategic Research Grant (SRG) Type C Scheme (Contract No. 1515/PKS/ITS/2026)

Funding
Institut Teknologi Sepuluh Nopember: Contract No. 1515/PKS/ITS/2026

Data availability
The data cannot be made publicly available upon publication because no suitable repository exists for hosting data in this field of study. The data that support the findings of this study are available upon reasonable request from the authors.

References

[1] Saqib M *et al.* 2024 "Designing of low band gap organic semiconductors through data mining from multiple databases and machine learning assisted property prediction" *Optical Materials* **150** 115295 doi:10.1016/j.optmat.2024.115295

[2] Biswas S 2022 "Determination of the band gap of germanium and silicon using ExpEYES-17 kit" *Physics Education*

[3] Biswas S and Roy D 2022 "Microcontroller based study of diode thermometers for online demonstration of undergraduate laboratory classes in COVID-19 lockdown" *Physics Education*

[4] Mitra S, Mishra A and Barua S 2022 "Arduino based temperature controlled sample holder using a power transistor and its application to measure the band gap of a silicon p–n diode" *European Journal of Physics* **43**(1) doi:10.1088/1361-6404/ac362d

[5] Valastro S *et al.* 2024 "Temperature-Dependent Excitonic Band Gap in Lead-Free Bismuth Halide Low-Dimensional Perovskite Single Crystals" *Advanced Optical Materials* **12**(11) doi:10.1002/adom.202302397

[6] Liu L, Xue D and Zhang S 2023 "General type industrial temperature system control based on fuzzy fractional-order PID controller" *Complex & Intelligent Systems* **9**(3) 2585–2597 doi:10.1007/s40747-021-00431-9

[7] Jia Y, Zhang R, Lv X, Zhang T and Fan Z 2022 "Research on Temperature Control of Fuel-Cell Cooling System Based on Variable Domain Fuzzy PID" *Processes* **10**(3) doi:10.3390/pr10030534

[8] Duman S, Gürbulak B and Şata M 2022 "Analysis of temperature dependent current-voltage characteristics of Sn/p-GaTe/In Schottky diode" *Optical Materials* **125** doi:10.1016/j.optmat.2022.112138

[9] Roogi J M and Devi M 2022 "Pre-current amplifier based transimpedance amplifier for biosensors" *International Journal of Reconfigurable and Embedded Systems* **11**(2) 188–195 doi:10.11591/ijres.v11.i2.pp188-195

[10] Iero D *et al.* 2021 "A technique for improving the precision of the direct measurement of junction temperature in power light-emitting diodes" *Sensors* **21**(9) doi:10.3390/s21093113

[11] Montgomery D C and Runger G C 2018 *Applied Statistics and Probability for Engineers* 7th edn (Hoboken, NJ: Wiley)

[12] Shilpa M K, Raheman M A, Aabid A, Baig M, Veeresha R K and Kudva N 2022 "A Systematic Review of Thermoelectric Peltier Devices: Applications and Limitations" *Fluid Dynamics and Materials Processing* **19**(1) 187–206 doi:10.32604/fdmp.2022.020351

[13] Rao C S, Santosh S and Dhanya Ram V 2020 "Tuning optimal PID controllers for open loop unstable first order plus time delay systems by minimizing ITAE criterion" *IFAC-PapersOnLine* **53** 123–128 doi:10.1016/j.ifacol.2020.06.021

[14] Wade H L 2004 *Basic and Advanced Regulatory Control: System Design and Application* (Research Triangle Park, NC: ISA)

[15] Chen J, Lu Q, Bai J, Xu X, Yao Y and Fang W 2021 "A temperature control method for microaccelerometer chips based on genetic algorithm and fuzzy PID control" *Micromachines* **12**(12) doi:10.3390/mi12121511

[16] Wang T, Wang H, Hu H, Lu X and Zhao S 2022 "An adaptive fuzzy PID controller for speed control of brushless direct current motor" *SN Applied Sciences* **4**(3) doi:10.1007/s42452-022-04957-6

[17] Cao W, Liu Z, Song H, Li G and Quan B 2024 "Dung Beetle Optimized Fuzzy PID Algorithm Applied in Four-Bar Target Temperature Control System" *Applied Sciences* **14**(10) doi:10.3390/app14104168

[18] Fiore J M 2021 *Semiconductor Devices: Theory and Application* 1st edn

[19] Shuvo M S, Ishtiaq F, Jamee T, Das J and Saha S 2022 "Analysis of internal cooling system in a vented cavity using P, PI, PID controllers" *Results in Engineering* **15** doi:10.1016/j.rineng.2022.100579

[20] Morab S, Sundaram M M and Pivrikas A 2023 "Review on Charge Carrier Transport in Inorganic and Organic Semiconductors" *Coatings* **13**(9) doi:10.3390/coatings13091657